FIV2024
IGUAÇU FALLS, BRAZIL
2-5 JULY 2024

FIV2024: FSI² & FIV + N
10th International Symposium on Fluid-Structure Interactions,
Flow-Sound Interactions, Flow-Induced Vibration & Noise

FIV2024-0062
Piezoelectric energy harvesting from VIV on cantilevered flexible cylinders with orthotropic bending stiffness: experimental investigation of varying flow effects

Letícia Siqueira Madi[1]
Guilherme Jorge Vernizzi[1]
Wagner Antonio Defensor Filho[1]
Andre M. Kogishi[2]
Celso P. Pesce[1]
1 – Offshore Mechanics Laboratory (LMO), Escola Politécnica, Universidade de São Paulo, Brazil
2 – Institute for Technological Research (IPT), São Paulo, Brazil
leticia.madi@usp.br, guilherme.jorge.lopes@usp.br, wadfilho@usp.com, amkogishi@ipt.br, ceppesce@usp.br

Abstract. *This study presents experimental tests of VIV over an orthotropically stiffened cantilevered cylinder, equipped with piezoceramic components over a flat bar in its interior. The displacements of the cantilever were measured using an optical system tracking reflective targets distributed along the model. Additionally, the resulting reaction forces and the electric tension output from the attached piezoelectric components were measured. The experimental campaign employed two methodologies: constant towing velocities until a steady state regime was reached, and constant low acceleration until the maximum towing velocity was reached, followed by deceleration at the same rate. The reduced velocities reached up to 20, which allowed for the exploration of various VIV frequencies and response branches. Modal decomposition using the Galerkin method is employed for data analysis, along with time and frequency domain techniques such as Fourier Transform and Hilbert-Huang Transform. The results indicate clear hysteretic behaviour of the system as modal responses transition between the amplitude response branches. The analysis and discussion of the electric power output are also addressed.*

Keywords: *Vortex-Induced Vibration, piezoelectric energy harvesting, experimental analysis, orthotropic stiffness, Hilbert-Huang transform.*

NOMENCLATURE AND DEFINITIONS

Dimensional parameters			
Stream velocity	U	Natural frequencies ($n = 1, 2, ...$)	f_{x_n} , f_{y_n}
Vortex shedding frequency	f_s	Mean forces	$\bar{F}_x$, $\bar{F}_y$
Cantilever diameter	D	Oscillatory forces	F_x , F_y
Cantilever length	L	Electrical resistance	R
Longitudinal and transverse displacements	x , y	Electric tension	V
Amplitudes of displacement	A_x , A_y	Mean electric power	$\bar{W}$
Frequencies of response	f_x , f_y		

Dimensionless parameters					
Strouhal number	S_t	$= f_s \dfrac{D}{U}$	Dimensionless amplitudes	A_x^* , A_y^*	$= \dfrac{A_x}{D}$, $\dfrac{A_y}{D}$
Reduced velocity	U_{r_n}	$= \dfrac{U}{f_{y_n} D} = \dfrac{f_s}{f_{y_n}} \dfrac{1}{St}$	Modal amplitudes	$A_{x_n}^*$, $A_{y_n}^*$	
Dimensionless displacements	x^* , y^*	$= \dfrac{x}{D}$, $\dfrac{y}{D}$	Dimensionless frequency	f_x^* , f_y^*	$= \dfrac{f_x}{fx_n}$, $\dfrac{f_y}{fy_n}$
Modal displacements	x_n , y_n				

1. INTRODUCTION

Energy harvesting from alternative power sources is a prominent area of technological research. Vortex-Induced Vibrations (VIV) have received considerable attention due to their self-excited and self-limited oscillations, which allow for controlled vibrations that can be converted into electrical energy. For instance, the VIVACE is a medium-power device that uses a configuration of tandem-arranged rigid cylinders coupled to electromagnetic transducers to generate electricity. For more information on the VIVACE, refer to Bernitsas *et al.* (2006) and Sun *et al.* (2017). Regarding low power generation, piezoelectric transducers are widely used for the conversion of mechanical energy into electricity. These harvesters are particularly useful for meeting the low-power requirements of self-reliant electronic devices such as remote sensors (Han *et al.* (2023)). Harvesters that utilize the VIV phenomenon with piezoelectric conversion have been documented in the works of Song *et al.* (2015), Shan *et al.* (2017), Han *et al.* (2020) and Zhao *et al.* (2022).

The classically studied VIV phenomenon on rigid cylinders, however, presents a practical obstacle to energy harvesting. The viability of the device is constrained within a small range of flow velocities in which the lock-in occurs, characterised by a narrow spectrum of operating frequencies, in addition to limited displacement amplitudes. This problem can be surpassed by alternative structural arrangements.

In the specific scenario of VIV occurring on a flexible cantilevered cylinder with a flat bar that imparts greater stiffness in the direction of flow than in the transverse one, an unconventional dynamic response branch with large amplitudes is observed at high reduced velocities. This distinctive behaviour, as initially documented by Fujarra *et al.* (2001), exhibits a high energy branch where desynchronisation would be expected in rigid cylinders under the phenomenon, as shown in Fig. 1. Experiments conducted by Defensor Fo. *et al.* (2022) confirm that this branch remains stable even at high inflow velocities, displaying a complex frequency spectrum with multimodal responses for configurations with different ratios between the longitudinal and transverse natural frequencies ($f_{x_1} : f_{y_1}$). Figure 2 shows the amplitude and frequency spectra for a model with a natural frequency ratio of $f_{x_1} : f_{y_1} = 2 : 1$, indicating the existence of multimodal responses at higher reduced-velocities in this type of structural arrangement, causing the so-called high-energy branch and leading to large amplitudes of displacements.

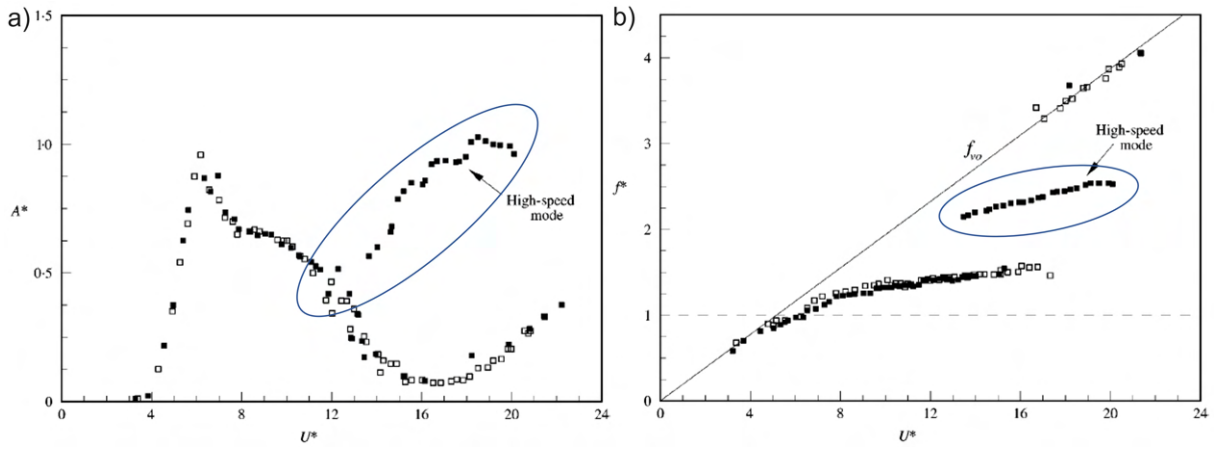

Figure 1. VIV response for orthotropic stiffened flexible cantilevered cylinder of $f_{x_1} : f_{y_1} = 4 : 1$: (a) dimensionless cross-wise amplitudes and (b) dimensionless frequency of vibration as functions of reduced velocity. (Fujarra *et al.*, 2001). High-speed mode branch highlighted.

Based on the results of these previous investigations, this study presents an energy harvester intended to exploit the high frequencies exhibited by this distinctive branch of the dynamic response. The harvester was tested experimentally using an orthotropically stiffened cantilever cylinder with piezoceramic components attached to the inner flat bar to convert vibrational energy into electricity.

2. EXPERIMENTAL SET-UP

The model under study, represented in Fig 3, is composed of a standard PVC pipe of length $L = 2.0$ m and external diameter $D = 40$ mm, cantilevered and stiffened orthotropically by an arrangement of internal flat bars. Piezoelectric layers are attached to both sides of the clamped end of the internal beams. These layers are macro fiber composites (MFC) from Smart Material Corporation®, made of piezoceramic fibers aligned and embedded in epoxy adhesive and a polymeric film, with electrodes attached. Each MFC connects to a basic electrical circuit with only an electric resistance of $R = 270$ kΩ in parallel. Table 1 lists structural and electric parameters relevant for the experiments, as well as the longitudinal and transverse natural frequencies determined by decay tests.

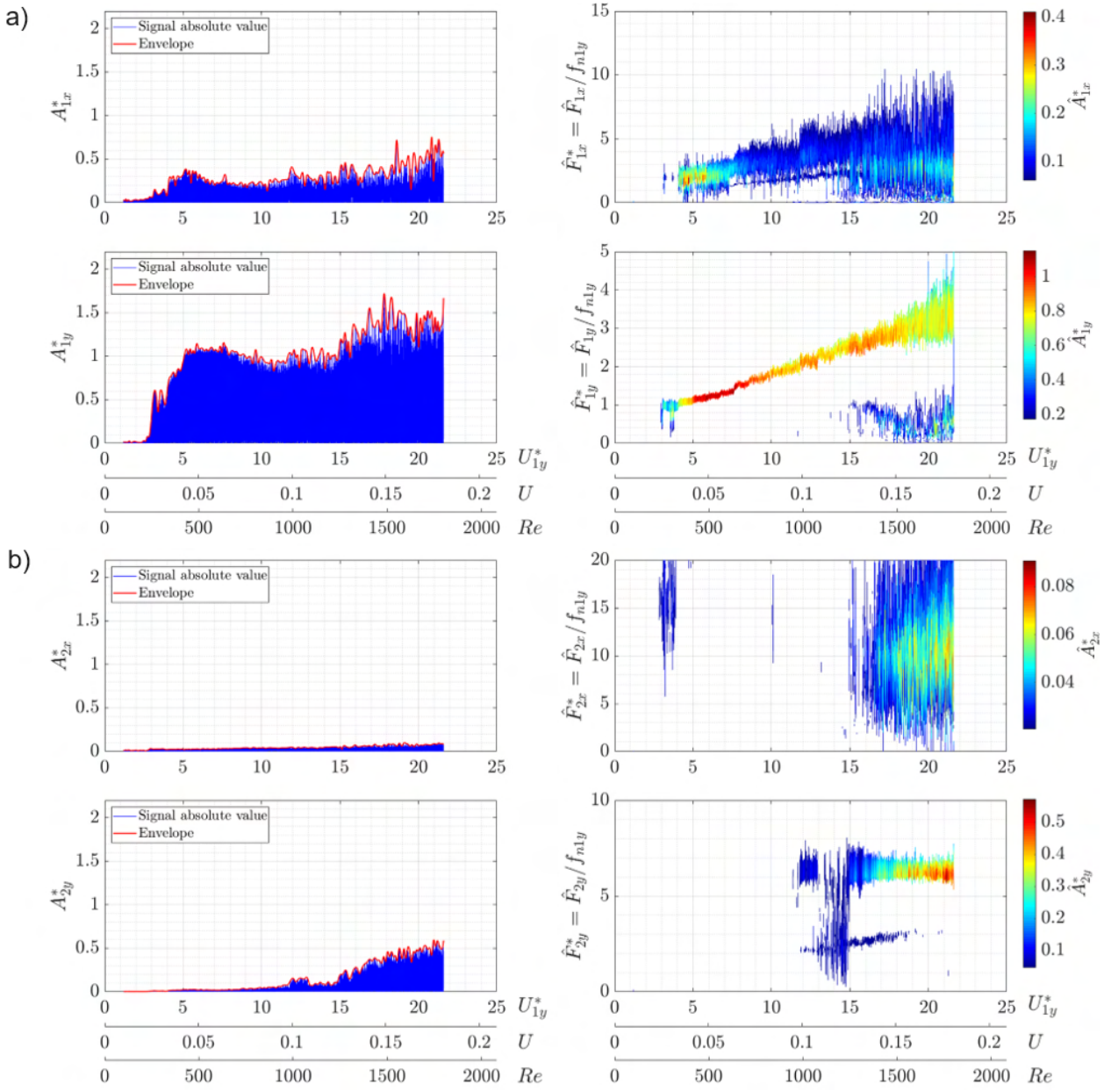

Figure 2. Modal VIV response branches for orthotropic stiffened flexible cantilevered cylinder: (a) first mode and (b) second mode in-line and cross-wise dimensionless modal amplitudes and dimensionless modal frequencies as functions of reduced velocity. Model nominal frequency ratio $f_{x_1} : f_{y_1} = 2 : 1$ (Defensor Fo. *et al.*, 2022).

Table 1. Parameters related to the experimental model

Structural parameters		**Natural frequencies**	
Length (L)	2.0 m	1st Longitudinal mode natural frequency (f_{x_1})	2.34 Hz
Diameter (D)	40 mm	1st Transverse mode natural frequency (f_{y_1})	1.32 Hz
Electrical resistance (R)	270 kΩ	2nd Transverse mode natural frequency (f_{y_2})	8.30 Hz
		Frequency ratio (f_{x_1}/f_{y_1})	1.77

The experiments were carried out at the towing tank facility of the Institute for Technological Research (IPT). The working section of the tank is 200 m long, 6 m wide and 3.8 m deep. The displacements were directly measured using Qualysis® underwater optical tracking system, which collected data from a set of reflective targets placed at equally spaced intervals along the model. The piezoelectric actuators utilized, the experimental model and the set-up of the camera system attached to the towing carriage is shown in Fig. 4. The reaction forces on the system were assessed by load cells placed at the clamped end of the model. The electric tension output of the piezoelectric circuits was also acquired.

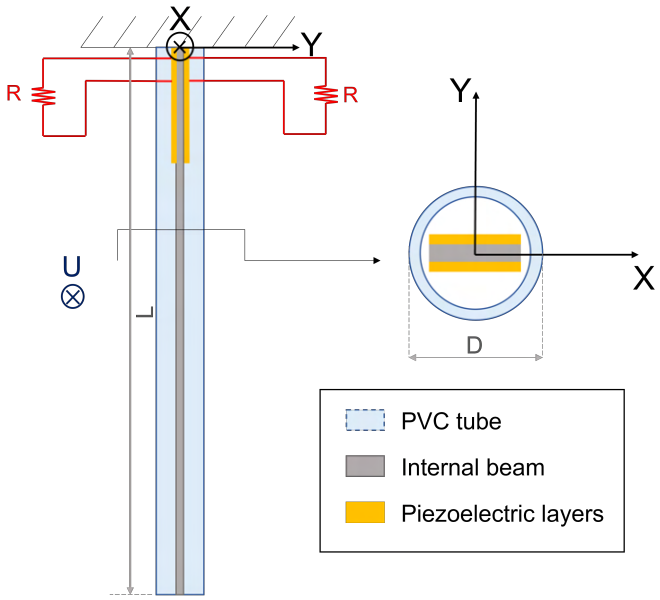

Figure 3. Schematic representation of the experimental model.

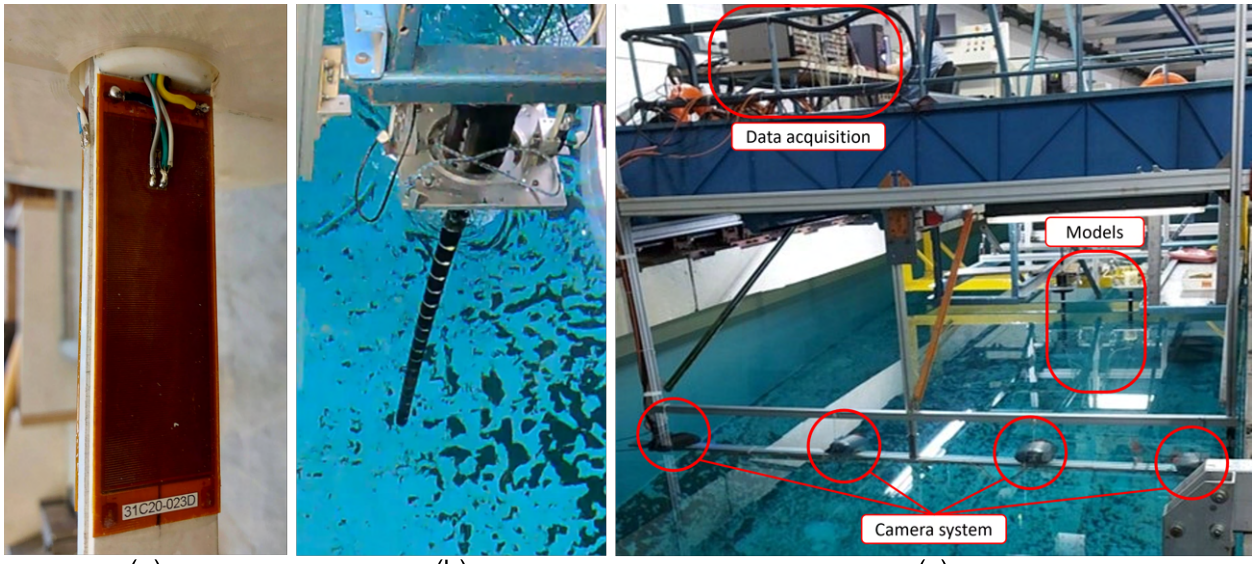

Figure 4. Experimental set-up: (a) MFC beam attached to the model and the electric circuit; (b) cantilevered model attached to the towing car structure in the water channel; (c) arrangement of the towing car in the IPT towing tank.

Two types of tests were conducted: *(i)* constant towing velocities (stepped speeds), and *(ii)* constant slow acceleration until a maximum velocity was reached, followed by deceleration at the same rate. For the first type, a set of 10 test velocities was defined at which the car was towed until a steady state response was reached. The towing velocities varied from $U = 0.1$ m/s to $U = 1.0$ m/s, at a stepped variation of $\Delta U = 0.1$ m/s. In the second type of tests, the carriage begins from a stationary position and accelerate at a rate of $a = 0.05$ m/s^2 until reaching the velocity of $U = 1.0$ m/s, followed by deceleration at the same rate. Three independent runs were performed for all tests of both types.

3. RESULTS AND DISCUSSION

The raw data are first subjected to an *ad hoc* pre-processing algorithm that restores lost signals and interpolates it to a more refined discretization along the model (see Defensor Fo *et al.* (2023); Vernizzi *et al.* (2023)). An initial study on the tests of type *(i)*, constant velocities, can be found in Madi *et al.* (2023).

3.1 Displacements

For a type *(ii)* test (slowly varying velocity), Fig. 5 shows time series of both the in-line and the crosswise displacements. The displacements measured at the free-end of the flexible cylinder (x^* and y^*, respectively) are normalized by the diameter of the model. Galerkin projection techniques were used for modal analysis, employing the Euler-Bernoulli cantilever modes as modal functions; see Blevins (2001). For each direction, Fig. 5 displays in the first chart the dimensionless tip displacement, while the next charts present, respectively, the modal displacements of the first, second and third natural modes of vibration. It is evident that, in both directions, the third mode has a very small contribution to the system displacements. On that note, the following analysis focuses on the first and second modes of response.

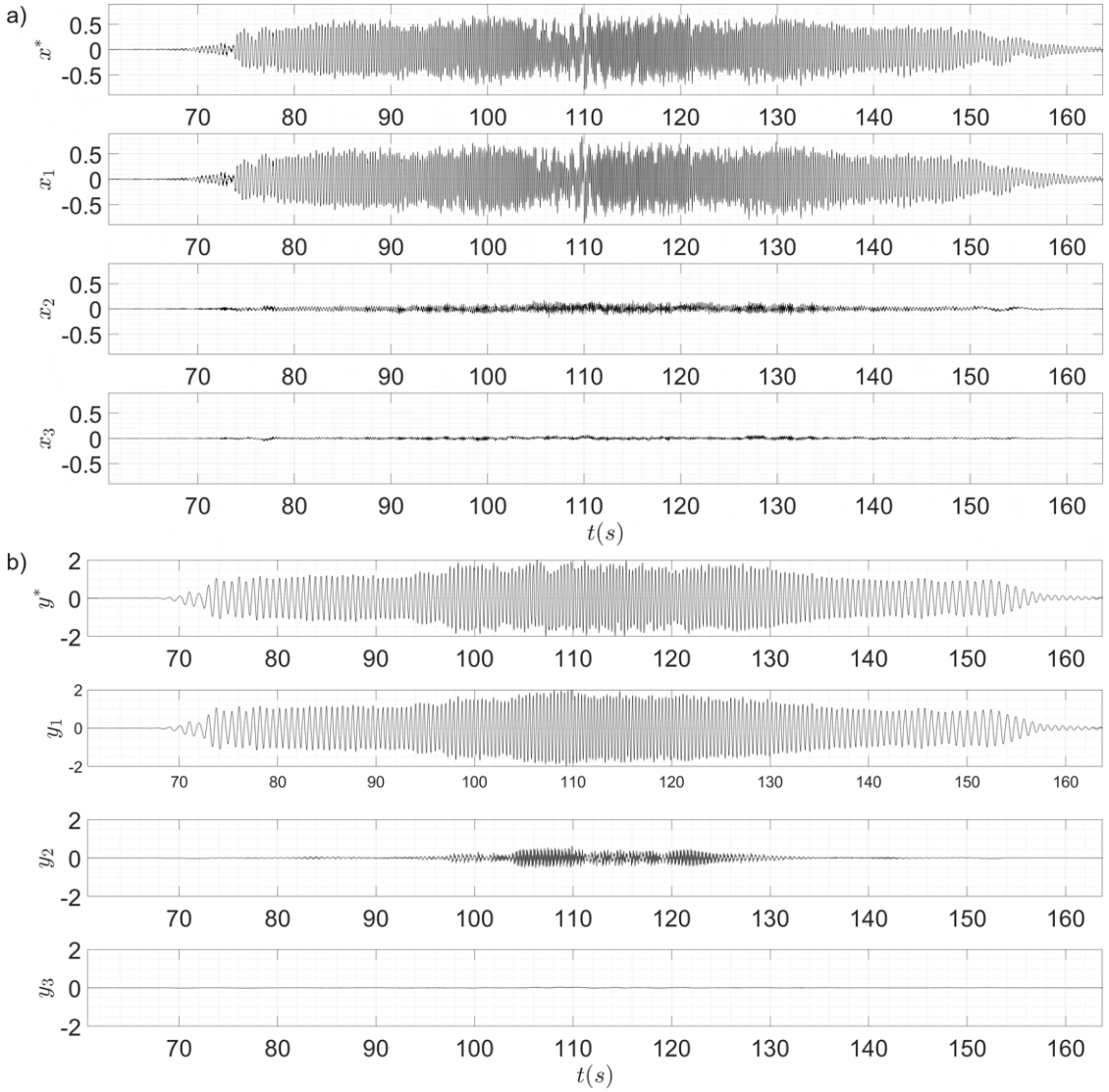

Figure 5. Time series of the displacements, in (a) longitudinal and (b) transverse direction, of the cantilever free-end normalized by the cylinder diameter (x^* and y^*) and modal components (x_1, x_2, x_3; y_1, y_2, y_3).

The amplitude of the stationary part of the time series for each constant velocity of the tests of type *(i)* is determined by taking into account the 10% of the highest peak values. For type *(ii)* tests, the envelope of the absolute value of the time series is calculated. The dimensionless in-line displacement amplitude at the tip of the model A_x^* and the crosswise displacement amplitude A_y^* are both shown in Fig. 6, where the amplitudes calculated for the steady-state series are compared with the envelope calculated for the type *(ii)* tests. The amplitude envelopes for increasing and decreasing velocities are shown in two distinct colors (blue and red). The in-line lock-in occurs synchronously with the transverse direction at approximately $Ur_1 = 7.5$. The shift of the in-line lock-in compared to a classical VIV response is attributed to the influence of the orthotropic stiffness ratio. The amplitudes of response remain increasing at high reduced velocities, reaching maximum amplitudes of $A_x^* = 0.5$ and $A_y^* = 2$. Furthermore, the results for the varying velocity tests indicate a hysteretic behaviour of the system, as separate paths between the amplitudes from increasing and decreasing velocities can be clearly identified.

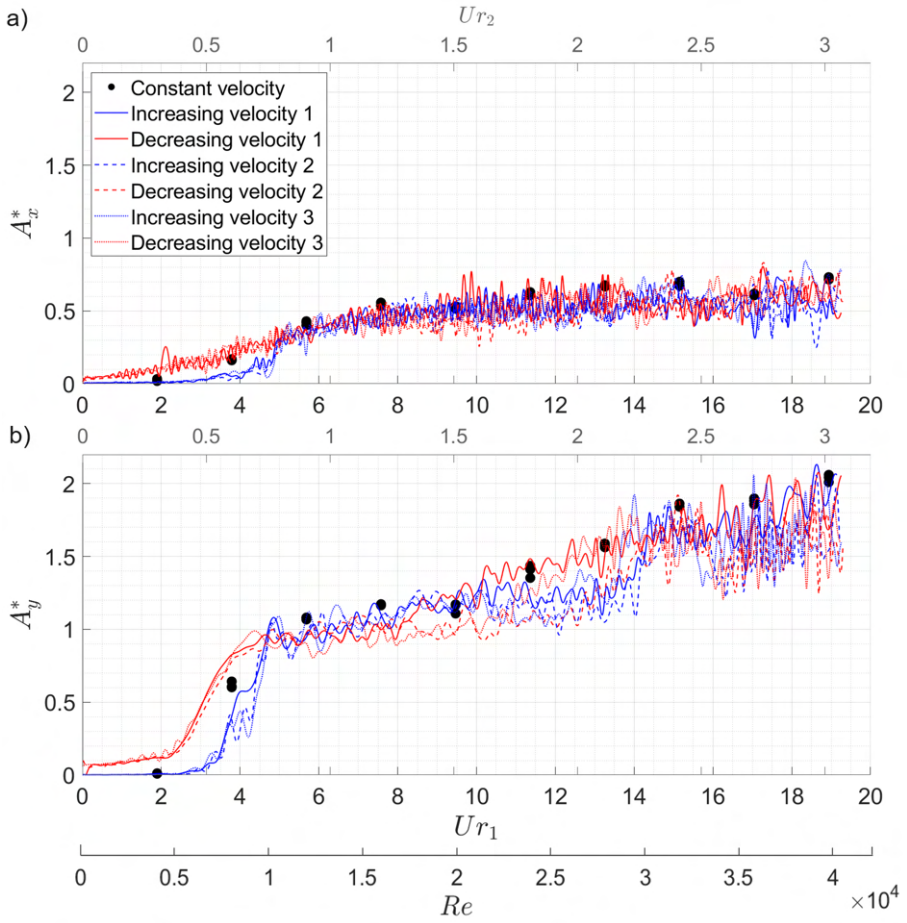

Figure 6. Dimensionless amplitudes of displacements for the cantilever end: (a) longitudinal displacements; (b) transverse displacements.

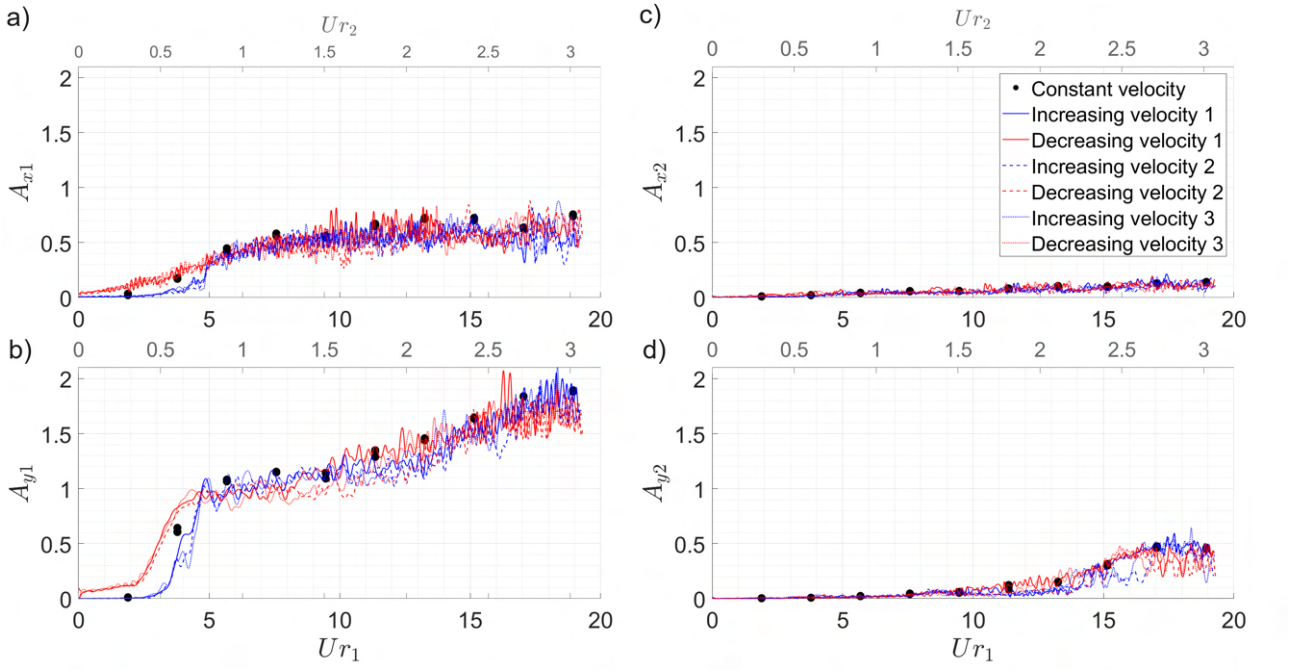

Figure 7. Modal amplitudes of displacements for the cantilever: (a) first longitudinal mode; (b) first transverse mode; (c) second longitudinal mode; (d) second transverse mode

Regarding the projected modal response, the first two modal amplitudes of displacements on both orthogonal directions, calculated analogously to the previous case, are presented in Fig. 7. The longitudinal response is predominantly composed by the first mode of vibration, while the transverse displacements show the first mode as mostly the only present until $Ur_1 = 10$, followed by a multimodal response, formed by the first mode upper branch and the second mode initial branch. This new synchronization begins at a reduced velocity calculated for the second mode of around $Ur_2 = 2$. The coexistence of different modes of vibration characterize the high-energy branch, which is therefore identified starting at $Ur_1 = 10$ onwards; see also Defensor Fo. *et al.* (2022). The modal responses exhibit the same hysteresis patterns as the cantilever tip displacements.

The frequency spectra for the first type of tests (constant velocities) are obtained using a Fast Fourier Transform (FFT), while the instantaneous frequencies of the second type are calculated by applying a Hilbert-Huang Transform (HHT); for detailed information on the HHT and its application in VIV analysis, refer to Huang *et al.* (1998) and Pesce *et al.* (2006). Figure 8 shows the dominant frequencies for each mode in both directions, f_x^* and f_y^*, normalized by the natural frequency in still water in the cross-wise direction (f_{y_1}). The marker size is proportional to the amplitude of response in that frequency. To ensure a clearer visual representation, the time-frequency spectra are sampled at reduced velocities near the constant velocities tested and at intermediate values. The dominant frequency of the system in both directions is close to the respective natural frequencies at reduced velocities from $Ur_1 = 4$ to $Ur_1 = 8$, which corresponds to the upper branch of response and the peak of lock-in of the VIV phenomenon for the first mode of vibration. A dual resonance is present as both the longitudinal and transverse first modes approach their respective natural frequencies within the same range of reduced velocities. From $Ur_1 = 10$ onwards (in the high-energy branch), the second mode of transverse vibration appears, with a dominant frequency of response close to its natural frequency value, which indicates the start of a second mode synchronization around $Ur_2 = 3$. Note, however, that the first mode remains the most influential in the response, presenting the greatest amplitudes even at higher reduced velocities.

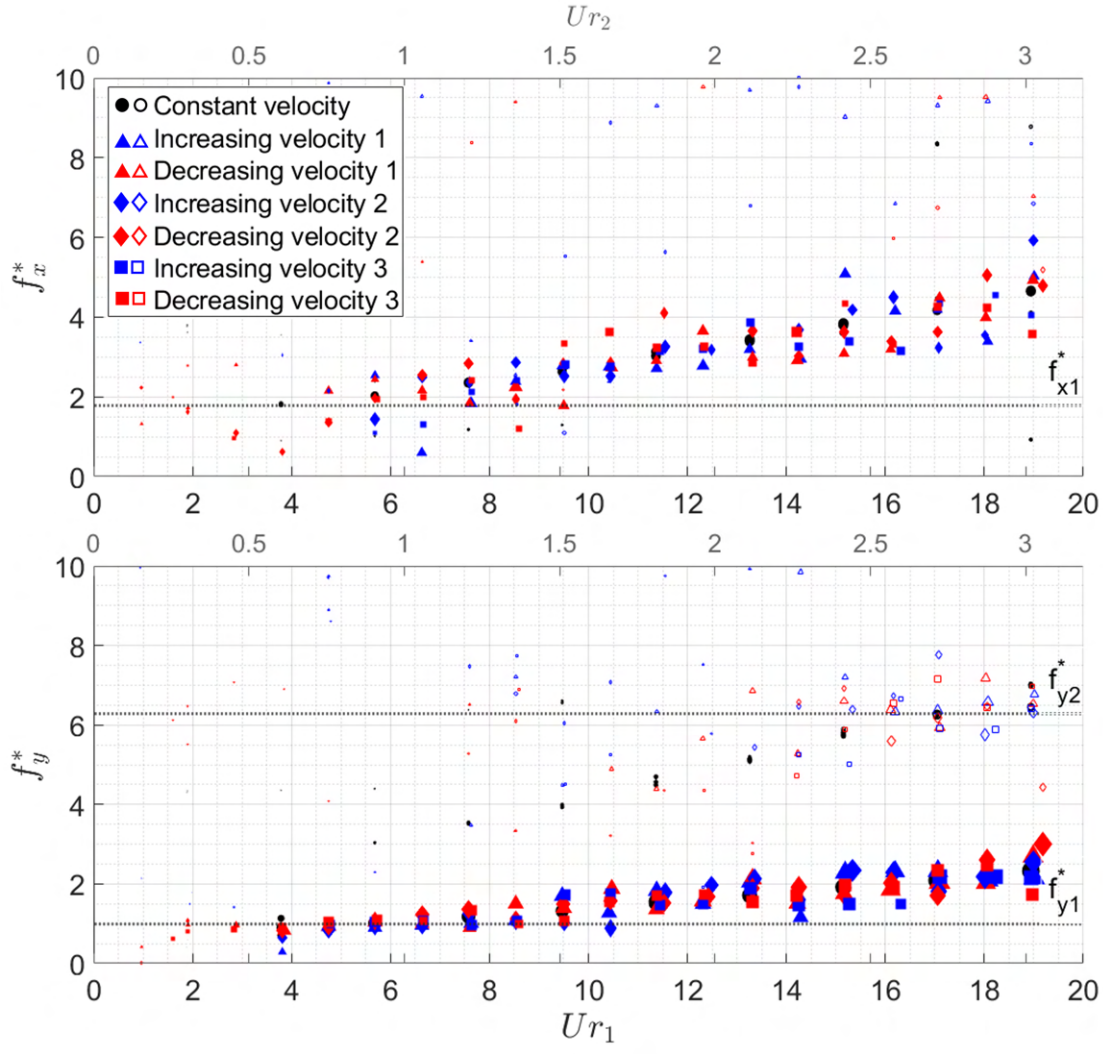

Figure 8. Modal dominant frequencies. Closed markers represent first mode frequencies, while open markers are second mode frequencies.

The response of the high-energy branch, observed in Figs. 7 and 8, is due to the cantilever orthotropic stiffness, as already established in Fujarra *et al.* (2001) and Defensor Fo. *et al.* (2022). This arrangement may therefore allow energy harvesting to be extended to a wide range of reduced velocities, where the oscillation frequencies are higher and associated with large amplitudes. Consequently, higher electrical power is implied, which is the premise of the concept under investigation.

3.2 Reaction forces

The reaction forces measured at the clamped end of the cantilever in both longitudinal and transverse directions are shown in Fig. 9. The mean value ($\bar{F}_x$ and $\bar{F}_y$) and amplitude of the oscillatory forces (F_x and F_y) are presented separately. For type *(ii)* tests, the mean value is obtained through the residue of the Empiric Modal Decomposition (EMD); see Pesce *et al.* (2006), Franzini *et al.* (2008) and Defensor Fo. *et al.* (2022) for EMD applications to VIV experiments. In the transverse direction, an asymmetry in the physical model is inferred as the mean force deviates from zero. For reduced velocities within the range of the upper branch of response, it can be observed that the order of magnitude of the amplitudes of the oscillatory part of the forces is similar for both directions. However, the crosswise force increases significantly within the high-energy branch, especially when multiple frequencies are involved. It is also noteworthy that the system exhibits a significant hysteresis response at reduced velocities from $Ur_1 = 15$ onwards.

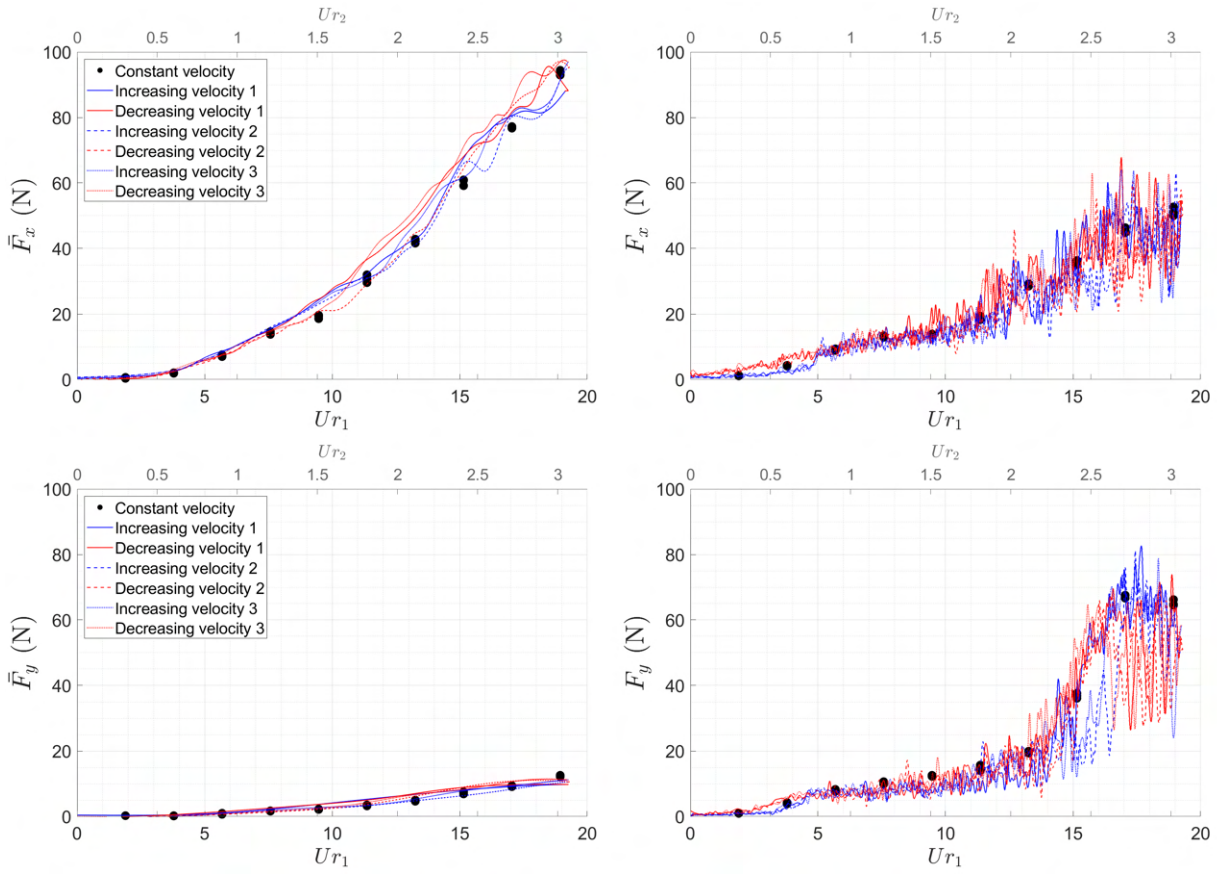

Figure 9. Mean and oscillatory parcels of the hydrodynamical forces in longitudinal and transverse directions.

3.3 Piezoelectric response

The piezoelectric sensors installed in the model are attached to separate electric circuits, each with independent electric tension measurements. Figure 10 shows the amplitude of the voltage output from each transducer. The difference between the responses V_1 and V_2 can be attributed to the structural asymmetry of the model, as indicated by the transverse force. The electric tension increase is significant within the velocity range where multiple frequencies occur; i.e., in the high-energy branch of response.

The estimation of the electric power harvested by the system was calculated by the mean electric power evaluated within a chosen time window t_0 to t_1 using the expression $\bar{W} = \left(\int_{t_0}^{t_1} \frac{V^2}{R} \mathrm{d}t \right) / (t_1 - t_0)$. The type *(i)* tests use the entire steady-state series as reference for the calculation. For type *(ii)* tests, a moving window is used to calculate the

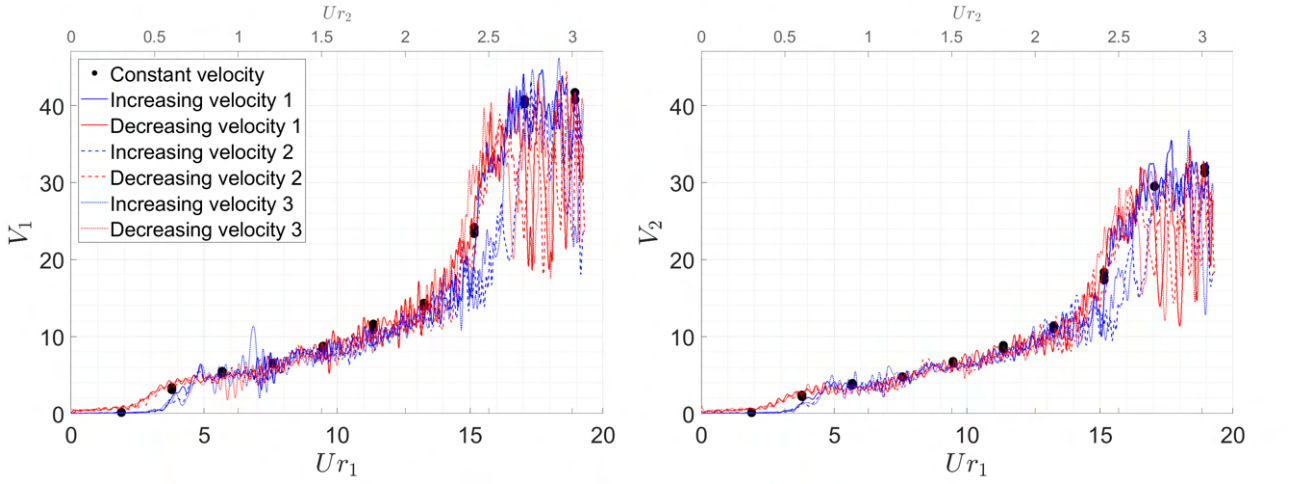

Figure 10. Electric tension harvested from the piezoelectric circuits.

mean power. This calculation considers one second before and after each point of measurement, ensuring at least two cycles of oscillation for each point of analysis within the lock-in range. The results of these calculations, adding the values obtained for both circuits, are shown in Fig. 11. In this experimental campaign, the maximum mean power is estimated to be $\bar{W} = 4.5$ mW for the case of increasing velocity, while the cases of decreasing and constant velocities reached $\bar{W} = 3.5$ mW, with the difference being another indication of the hysteretical behaviour developed.

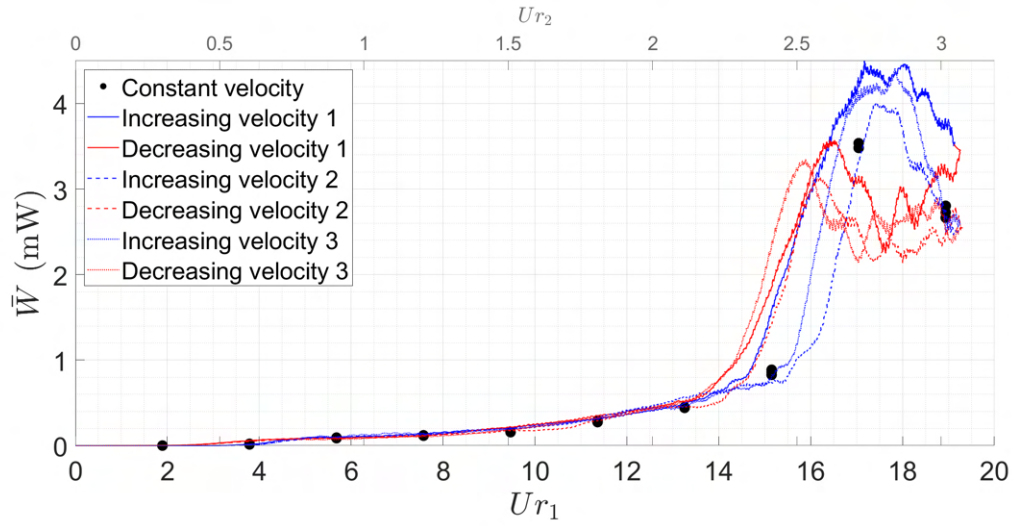

Figure 11. Electric power harvested.

4. CONCLUDING REMARKS

This experimental study compares VIV experiments with flexible cylinders exhibiting orthotropic bending stiffness using two methods: constant velocity and varying velocity with constant acceleration. The tests confirmed the existence of a high-energy branch at high reduced velocities, composed of various response modes and a diverse frequency spectrum. The occurrence of the high-energy branch was observed in both types of tests, in all independent runs. The slowly varying velocity tests revealed a hysteretic behaviour of the system. Maximum free-end transverse amplitudes over $A_y^* = 2$ were obtained with this configuration.

The tests also explored the potential of harnessing energy from VIV using piezoelectric components, and the viability of extracting electrical power especially from the so-called high-energy branch. The electric tension output of the piezoelectric circuits exhibited a multi-frequency nature, indicating the complex electrical response of the system. The voltage and the longitudinal reaction force at the clamped end are qualitatively similar, both showing a sharp increase in amplitude at reduced velocities over $Ur_1 = 15$, where multiple frequencies of response coexist. The estimation of the electric power harvested from the system demonstrated a maximum mean power output of $\bar{W} = 4.5$ mW for increasing velocity, while cases of decreasing and constant velocity reached $\bar{W} = 3.5$ mW.

The present experimental investigation serves as a proof-of-concept study, demonstrating the potential to convert vibrational energy from the high-energy branch observed in VIV experiments with the proposed structural configuration into electrical energy. The findings contribute to the understanding of the system dynamics and provide a basis for future optimisation of the energy conversion system. A patent request on this concept is already in progress.

ACKNOWLEDGEMENTS

L. Madi and W. Defensor Fo acknowledge their PhD scholarships, supported by the CAPES social demand, through the Graduate Program in Naval and Ocean Engineering (PPGEN). C.P. Pesce acknowledges the Brazilian National Council for Scientific and Technological Development for the research grant 307995/2022-4. Acknowledgements also to IPT for the support given to L. Madi through its Young Talent Program. The Sao Paulo Research Foundation (FAPESP) thematic project 'Nonlinear Dynamics Applied to Engineering Systems', process 2022/00770-0, is also acknowledged.

REFERENCES

Bernitsas, M.M., Raghavan, K., Ben-Simos, Y. and Garcia, E.M.H., 2006. "VIVACE (Vortex Induced Vibration Aquatic Clean Energy): A new concept in generation of clean and renewable energy from fluid flow". In *Proceedings of OMAE2006 - International Conference on Offshore Mechanics and Artic Engineering*.

Blevins, R.D., 2001. *Formulas for Natural Frequency and Mode Shape*. Krieger Pub Co. ISBN 1-57524-184-6.

Defensor Fo., W.A., Franzini, G.R. and Pesce, C.P., 2022. "An experimental investigation on the dual-resonance revealed in the VIV of flexible cantilevers with orthotropic bending stiffness". *Applied Ocean Research*, Vol. 126, p. 103263. doi:10.1016/j.apor.2022.103263.

Defensor Fo, W.A., Pesce, C.P., Vernizzi, G. and Maciel, V.S.F., 2023. "Experimental insights on the dynamics of submerged flexible pipes discharging water in post-critical regime". In *Proceedings of the XIX International Symposium on Dynamic Problems of Mechanics*. ABCM. doi:10.26678/abcm.diname2023.din2023-0115.

Franzini, G.R., Pereira, A.A.P., Fujarra, A.L.C. and Pesce, C.P., 2008. "Experiments on viv under frequency modulation and at constant reynolds numbers". In *Volume 5: Materials Technology; CFD and VIV*. ASMEDC, OMAE2008. doi:10.1115/omae2008-57957.

Fujarra, A., Pesce, C., Flemming, F. and Williamson, C., 2001. "Vortex-induced vibration of a flexible cantilever". *Journal of Fluids and Structures*, Vol. 15, pp. 651–658.

Han, P., Huang, Q., Pan, G., Qin, D., Wang, W., Gonçalves, R.T. and Zhao, J., 2023. "Optimal energy harvesting efficiency from vortex-induced vibration of a circular cylinder". *Ocean Engineering*, Vol. 282, p. 114869. doi:10.1016/j.oceaneng.2023.114869.

Han, P., Pan, G., Zhang, B., Wang, W. and Tian, W., 2020. "Three-cylinder oscillator under flow: Flow induced vibration and energy harvesting". *Ocean Engineering*, Vol. 211, p. 107619. doi:10.1016/j.oceaneng.2020.107619.

Huang, N.E., Shen, Z., Long, S.R., Wu, M.C., Shih, H.H., Zheng, Q., Yen, N.C., Tung, C.C. and Liu, H.H., 1998. "The empirical mode decomposition and the hilbert spectrum for nonlinear and non-stationary time series analysis". *Proceedings of the Royal Society of London. Series A: Mathematical, Physical and Engineering Sciences*, Vol. 454, No. 1971, pp. 903–995. ISSN 1471-2946. doi:10.1098/rspa.1998.0193.

Madi, L., Filho, W.A.D., Vernizzi, G., Kogishi, A.M. and Pesce, C.P., 2023. "Experimental assessment of piezoelectric energy harvesting from viv on cantilevered flexible cylinders with orthotropic bending stiffness". In *Proceedings of the 27th Brazilian Congress of Thermal Sciences and Engineering - COBEM2023*.

Pesce, C.P., Fujarra, A.L.C. and Kubota, L.K., 2006. "The hilbert-huang spectral analysis method applied to viv". In *Volume 4: Terry Jones Pipeline Technology; Ocean Space Utilization; CFD and VIV Symposium*. ASMEDC, OMAE2006. doi:10.1115/omae2006-92119.

Shan, X., Deng, J., Song, R. and Xie, T., 2017. "A piezoelectric energy harvester with bending–torsion vibration in low-speed water". *Applied Sciences*, Vol. 7, No. 2, p. 116. doi:10.3390/app7020116.

Song, R., Shan, X., Lv, F., Li, J. and Xie, T., 2015. "A novel piezoelectric energy harvester using the macro fiber composite cantilever with a bicylinder in water". *Applied Sciences*, Vol. 5, No. 4, pp. 1942–1954. doi:10.3390/app5041942.

Sun, H., Ma, C., Kim, E.S., Nowakowski, G., Mauer, E. and Bernitsas, M.M., 2017. "Hydrokinetic energy conversion by two rough tandem-cylinders in flow induced motions: Effect of spacing and stiffness". *Renewable Energy*, Vol. 107, pp. 61–80. doi:10.1016/j.renene.2017.01.043.

Vernizzi, G.J., Maciel, V.S.F., Defensor Fo., W.A., Orsino, R.M.M., Franzini, G.R. and Pesce, C.P., 2023. "Dynamic small-scale riser model experiments: a physics-based algorithm to recover lost measurements from optical tracking systems." In *Proceedings of the 42nd International Conference on Ocean, Offshore and Arctic Engineering - OMAE 2023*. Melbourne, Australia.

Zhao, J., Thompson, M.C. and Hourigan, K., 2022. "Damping effect on transverse flow-induced vibration of a rotating circular cylinder and its implied energy harvesting performance". *Physical Review Fluids*, Vol. 7, No. 2, p. 023905. doi:10.1103/physrevfluids.7.023905.